Source Process of the 1994 Far East Off Sanriku Earthquake, Japan, as Inferred from a Broad-Band Seismogram

Tôhoku Geophys. Journ. (Sci. Rep. Tôhoku Univ., Ser. 5), Vol. 34, No. 4, pp. 121-134, 1996

Source Process of the 1994 Far East Off Sanriku Earthquake, Japan, as Inferred from a Broad-Band Seismogram

TAKESHI NISHIMURA, HISASHI NAKAHARA, HARUO SATO
and MASAKAZU OHTAKE

Department of Geophysics, Graduate School of Science,
Tohoku University, Sendai 980-77

(Received November 7, 1995)

Abstract: The 1994 far east off Sanriku earthquake (Mw=7.7; the 1994 Sanriku-Oki earthquake) took place near the Japan trench on December 28, 1994. The earthquake was a reverse fault type, and the rupture proceeded westward to the Sanriku coast along the boundary between the Pacific plate and the landward plate, overlapping the southern part of the source region of the 1968 Tokachi-Oki earthquake (Ms=7.9). The Sanriku-Oki earthquake was well recorded without saturation by a broad-band seismometer (STS-2) at a station 300 km far from the epicenter. Fitting synthetic seismograms to the low-frequency component of the observed three-component waveform, we estimate slip distribution of the rupture on the main fault with an area of approximately 170 km×84 km. The fault mainly slipped in the region from the middle to the western (landward) part of the fault plane, having the maximum slip of 1.2 m, whereas a small slip of less than 0.4 m slip is observed in the region close to the initial break point. The total seismic moment amounts to 3.2×10^{20} Nm. The spatial distribution of fault slip indicates that the 1994 Sanriku-Oki earthquake ruptured the region of incomplete slip at the time of the 1968 Tokachi-Oki earthquake. From the analysis of the high-frequency component of the observed seismogram, we find that the high-frequency energy is also strongly radiated from the middle to the western part, with the highest intensity at the western edge of the fault plane. Most of the aftershock are observed outside the region of large slip at the time of the main shock.

1. Introduction

At 12h19m of 28 December 1994 (UT), a large earthquake of Mw=7.7 occurred far east off the Sanriku coast, northeast Japan. The Harvard CMT solution shows a focal mechanism of reverse fault type with a strike of 184°, a dip of 15° and a rake of 70° with a centroid at 143.12°E, 40.41°N, 34 km in the depth, suggesting that the earthquake ruptured along the boundary between the Pacific plate and the landward one. The epicenter of the main shock is located by the Japan Meteorological Agency at 143.43°E, 40.27°N, close to the Japan Trench, and most part of the aftershocks distribute in a region of about 170 km×84 km to the west of the initial break of the main event as shown in Figure 1. Umino *et al.* (1995) re-determined the focal depths for selected aftershocks accurately by using arrival times of depth phases (sP), and revealed that these events distribute along the boundary of the two plates. Matsuzawa *et al.* (1995) determined the focal mechanisms of the aftershocks from the initial motion of P-waves,

and observed larger dip angles (45°) for the aftershocks occurring close to the Sanriku coast. These results indicate that the rupture of the main shock proceeded westward from the trench axis along the plate boundary.

Seismogram of the main shock was completely recorded with a broad-band seismometer (STS-2) at the Tuyama station of the Department of Geophysics, Tohoku University, which is located about 300 km to the southwest of the epicenter (Figure 1). The seismic signals are digitized with a resolution of 24 bits and a sampling frequency of 80 Hz by using the Q680 system of QUANTERRA Inc. Figures 2 and 3 show the displacement record for three components, and filtered velocity seismograms for vertical component, respectively. Broad-band seismograms at other stations in the northeastern part of Japan were all saturated at the maximum amplitude (Matsuzawa, personal communication), and Tuyama is the closest station that recorded full broad-band waveform of the main shock.

The 1994 Sanriku-Oki earthquake took place within the area enclosed by the rupture zone of the 1968 Tokachi-Oki earthquake (Ms=7.9), whose source process was studied by Mori and Shimazaki (1985) and others. Hence, quantitative study on the source process of the 1994 Sanriku-Oki earthquake is important not only to understand the rupture process of this event but also to clarify its relation to the Tokachi-Oki earthquake of 26 years before. In the present study, we reveal the spatial distributions of fault slip and intensity of high-frequency wave radiation based on the broad-band seismogram observed at the Tuyama station. We further discuss the result in comparison with the aftershock distribution and the focal process of the 1968 Tokachi-Oki earthquake.

2. Slip Distribution

2.1. Fault Model and Inversion Method

We estimate the rupture velocity, rise time and spatial distribution of moment release for the main shock by fitting the synthetic displacement waveform with the observed one. The rectangle of 170 km×84 km in Fig. 1, which includes most part of the aftershocks, presents the horizontal projection of the rupture plane we assumed. The plane dips to the west following the distribution of well-relocated aftershock hypocenters (Umino *et al.*, 1995). We divide the rupture area into eight subfaults of roughly 40 km in the linear dimension so that each subfault is approximated by a point source at frequencies lower than 0.05 Hz. For all the subfaults, we fix the angles of strike and rake at 184° and 70°, respectively, following the CMT solution. The dip angle is changed in accordance with the location of subfaults referring to the spatial distribution of relocated aftershocks (Umino *et al.*, 1995) and the focal mechanisms of aftershocks (Matsuzawa *et al.*, 1995). The dip angles and depths of subfault at the center for the eight subfaults are summarized in Table 1.

We postulate that the rupture proceeds unilatelaly from the east to the west after the initial break at the subfault 8. We further assume a constant rupture velocity v_r, along

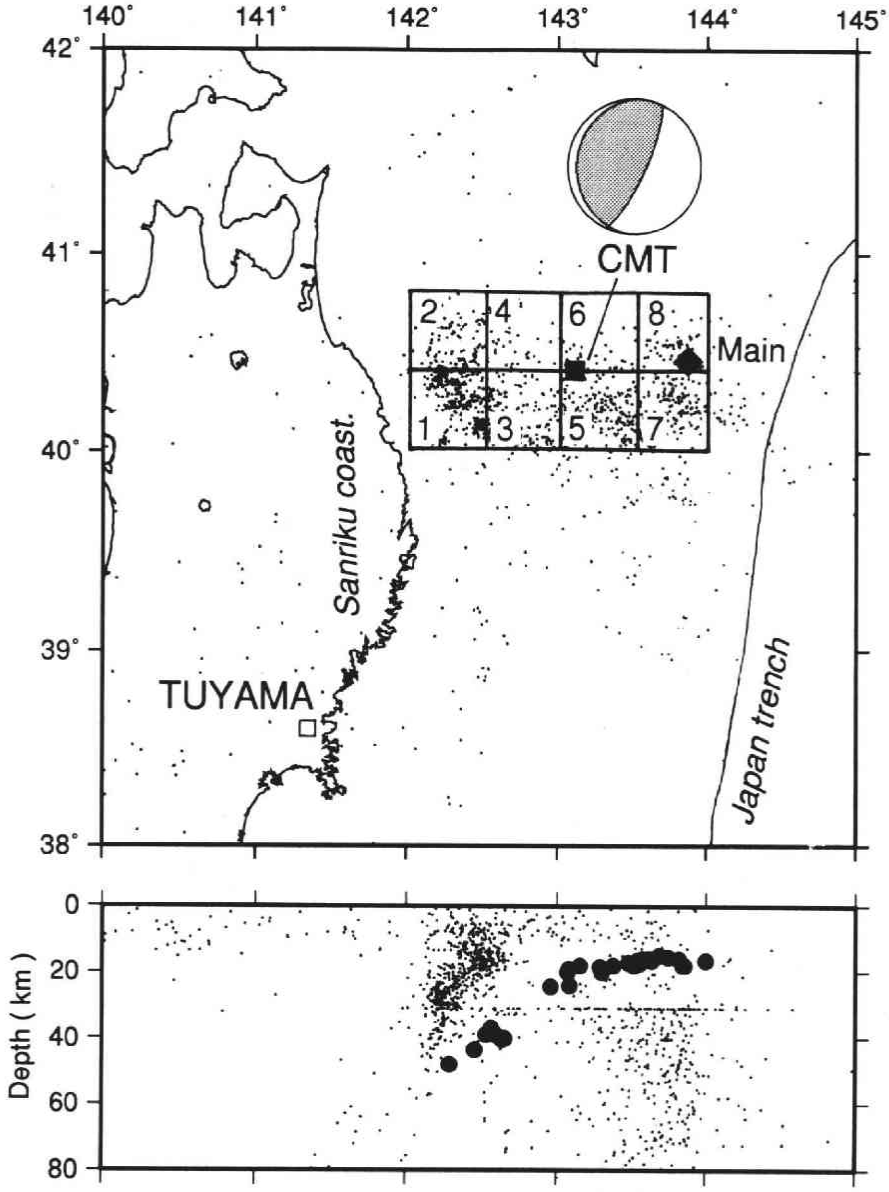

Fig. 1. Hypocenters of the 1994 Sanriku-Oki earthquake (diamond) and aftershoks for the period of Dec. 28, 1994-Jan. 10, 1995 (small dots), the fault area, the CMT solution by Harverd University (solid square is the centroid). Solid circles in the lower panel are re-determined hypocenters of selected aftershocks by Umino *et al.* (1995). Tuyama station is shown by open square. Rupture area of the main shock (approximately 170 km×84 km) is divided into eight subfaults for the analysis. Hypocenter locations are provided from the Observation Center for Prediction of Earthquakes and Volcanic Eruptions (OCPEV), Tohoku University.

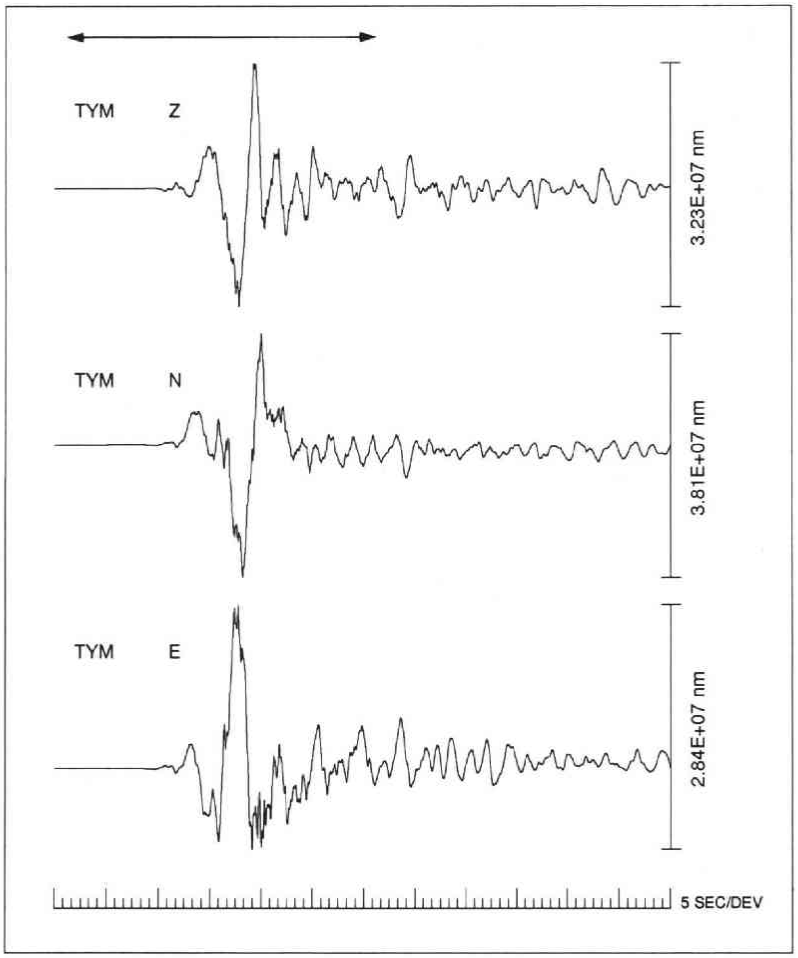

Fig. 2. Displacement seismogram of three components recorded by the STS-2 seismometer at the Tuyama station. Arrow indicates the data span used for the analysis of slip distribution.

the fault plane. The starting time of rupture for the k-th subfault, t_k^s, is calculated from the rupture velocity and the distance between the k-th subfault and subfault 8. A ramp function having a rise time τ is assumed as the source time function for all of the subfaults. The i-th component of the synthetic displacement seismogram, $C_i(t)$, can be expressed as

$$C_i(t_j\,;\,v_r,\tau)=\sum_{k=1}^{8} m_k G_{i,k}(t_j) * S(t_j\,;\,v_r,\tau), \tag{1}$$

where m_k represents the amount of moment release from the k-th subfault, i the component of seismogram, j the discrete time, $G_{i,k}(t_j)$ the Green's function for the i-th component by the k-th subfault, and $S(t_j)$ the source time function. Asterisk represents

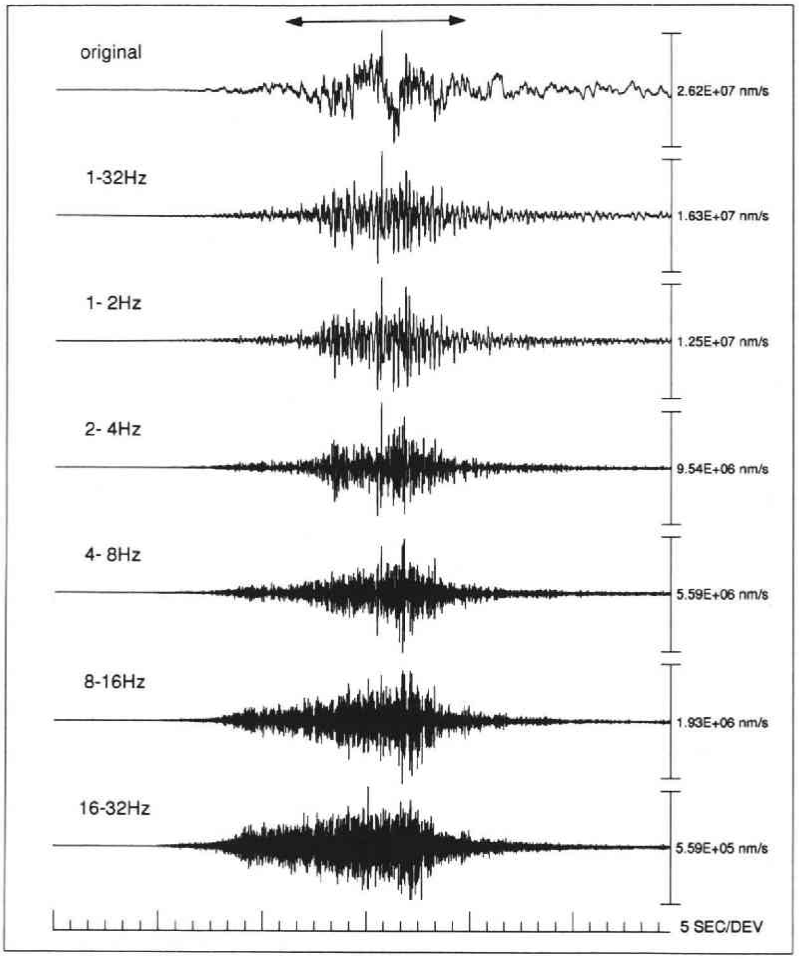

Fig. 3. Filtered velocity seismograms for vertical component recorded by the STS-2 seismometer at the Tuyama station. Arrow denotes the data span for the analysis of the radiation intensity of high-frequency waves.

Table 1. Elements of subfaults for the 1994 Sanriku-Oki earthquake

Subfault No.	Depth (km)	Dip (deg.)	Moment ($\times 10^{20}$ Nm)	Slip (m)	Resolution
1	51	32	0.25	0.2	0.69
2	51	32	−0.04	0.0	0.88
3	32	25	0.78	0.8	0.76
4	32	25	1.20	1.2	0.40
5	20	19	0.25	0.3	0.69
6	20	19	0.59	0.6	0.85
7	16	12	0.04	0.0	0.77
8	16	12	0.18	0.2	0.96

the convolution integral. We determine m_k ($k=1, \ldots, 8$) by minimizing a squared error, defined by

$$E^2(v_r,\tau)=\sum_{i=1}^{3}\sum_{j=1}^{n}[O_i(t_j)-C_i(t_j;\ v_r,\ \tau)]^2 \tag{2}$$

where $O_i(t)$ is the i-th component of the observed displacement and n is the total number of waveform data for each component.

We calculate the Green's functions for each subfault by using the discrete wavenumber method (Bouchon, 1981) and the reflection and transmission matrixes (Kennett and Kerry, 1979), assuming a horizontally layered structure with four layers as shown in Table 2 referring to Nishizawa *et al.* (1992). For the inversion, we use the three-component waveform data of 180 s (see Fig. 2) by resampling the data with a sampling frequency of 1 Hz. For smoothing the waveform, the second-order butterworth filter with a pass band of 0.05-0.01 Hz is applied both to the observed displacement and the synthetic one. Giving the rupture velocity v_r ranging from 2.0 to 3.8 km/s and the rise time τ from 4 to 16 s, which are common to all the subfaults, we estimate eight unknown parameters (m_k) from 540 points of waveform data. After the inversion for each v_r and τ, we choose the solution having the minimum residual as the best-fit solution.

2.2. Result

Figure 4 shows the distribution of the residual for different v_r and τ values, in which the residual is normalized by the minimum value. It is found from the figure that the rupture velocity of 3.0 km/s and the rise time of 10 s best fit the observed data. Figure 5 compares the observed waveforms with the best-fit synthetics. The synthetics well explain the characteristics of the main phases.

In Table 1, we summarize the result for each subfault with diagonal components of the resolution matrix in the inversion. Total moment release is estimated at 3.2×10^{20} Nm, which is in good agreement with 4.0×10^{20} Nm of the CMT solution by Harvard University. Slip d_k for each subfault is estimated from the relation $m_k=\mu d_k s_k$, where s_k is the area of the k-th subfault, and a rigidity of $\mu=5.0\times10^{10}$ N/m^2 is assumed. Average slip of the fault is estimated at 0.4 m, and the maximum one amounts to 1.2 m, which appears at the subfault 4. The regions having larger slip (subfault 3, 4, 6) are

Table 2. Horizontally layered structure for calculating the Green's function

Layer No.	Vp (km/s)	Vs (km/s)	Density (g/cm^3)	Thickness (km)
1	3.8	2.2	2.2	4
2	4.8	2.8	2.5	4
3	5.7	3.3	3.1	6
4	6.8	3.9	3.2	5
5	8.1	4.7	3.3	∞

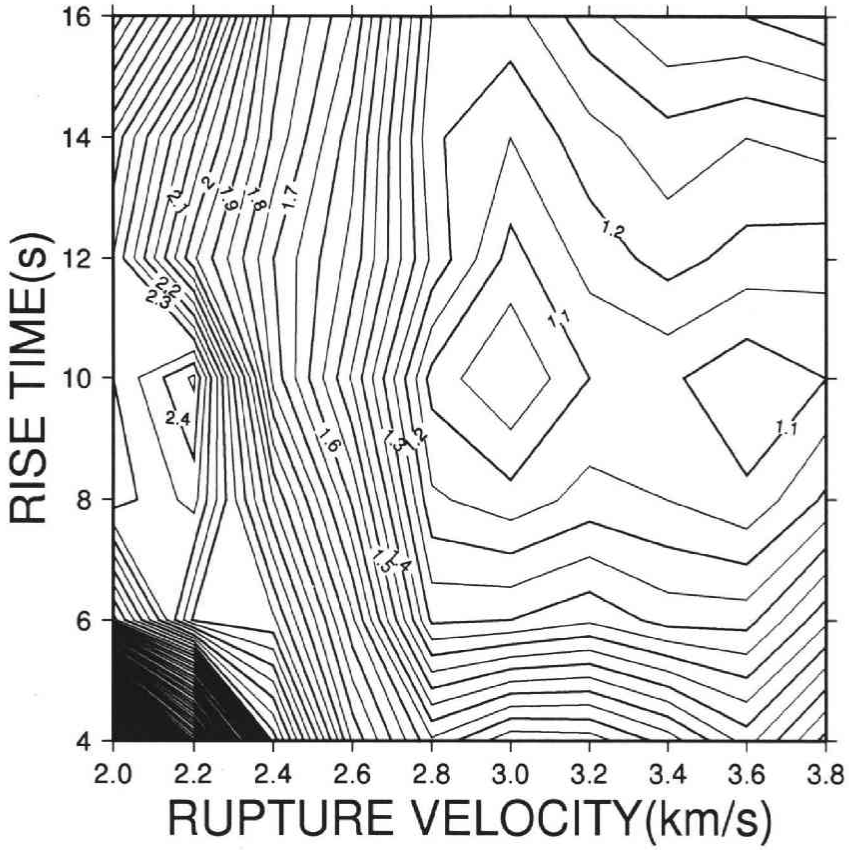

Fig. 4. Contour map of residuals as defined in eq. (2) for various sets of rupture velocity and rise time of the source time function.

observed in the middle to the landward part of the fault plane, which is consistent with the location of the CMT centroid. On the other hand, the region around the initial break point (subfault 7 and 8) and the western edge of the fault (subfault 1 and 2) slipped less than 0.4 m. We note that the portions of larger slip coincide with the turning point of the curvature of the plate boundary (see Fig. 1).

3. Spatial Distribution of High Frequency Wave Radiation

3.1. Method

We estimate spatial distribution of high-frequency wave radiation on the fault plane from the envelope of squared ground velocity. First, we assume that the high-frequency waves are mainly composed of far-field S-waves. We further assume the fault geometry and the rupture velocity as estimated in the preceding section, and calculate isochrones of the arrival time of the observed envelope. The isochrone shows which area of the fault plane contributes to each time on the observed seismogram (e.g., Spudich and

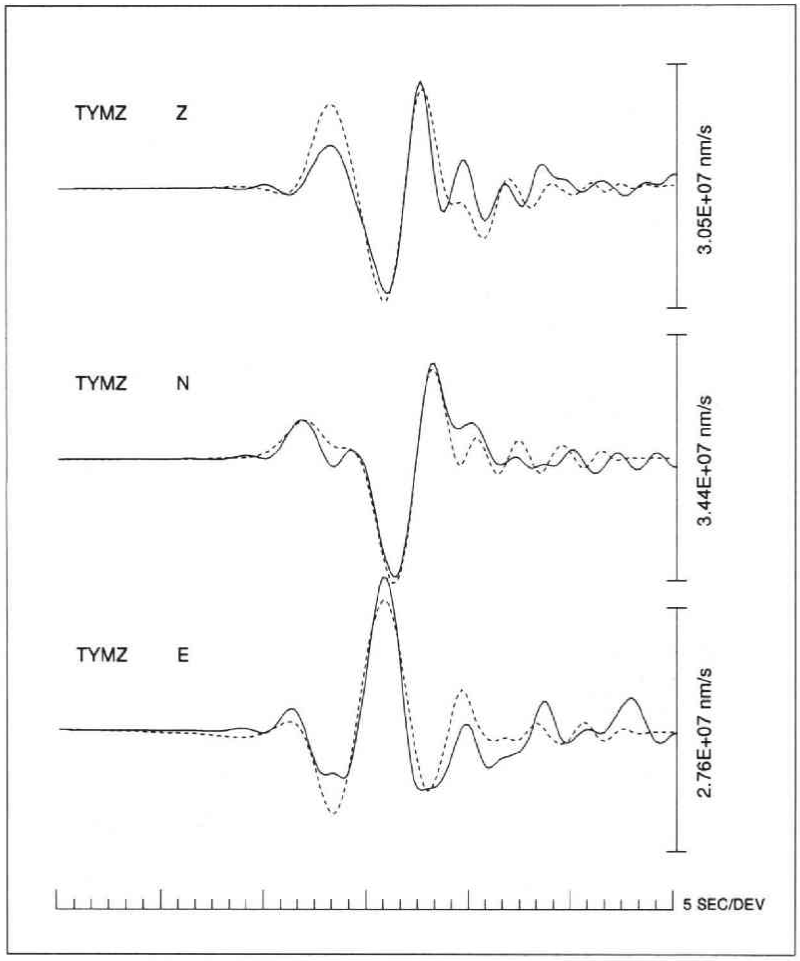

Fig. 5. Comparison between the observed (solid curves) and the synthetic (broken curves) seismograms of the 1994 Sanriku-Oki earthquake.

Frazer, 1984), and the envelope seismogram consists of waves radiated from subareas on the isochrone. We can express it as

$$\dot{u}^2(t)=\sum_{l=1}^{N}\left(R_l^{FS}\frac{r_a}{r_l}\right)^2 e_l\delta(t-t_l), \tag{3}$$

where $\dot{u}^2(t)$ is the summation of three-component squared velocity amplitude and δ is a delta function. l represents the subarea number, each of which have a unit area on the fault. Energy radiation intensity e_l shows the radiation intensity on the fault. t_l is the time when an isochrone intersects the l-th subarea, R_l^{FS} the radiation pattern of S-waves, and r_l the hypocentral distance, all of which are given from the fault geometry, the focal mechanism, and the rupture velocity that were estimated in the preceding section. N represents the total number of subarea, and r_a the arbitrary reference distance. Since

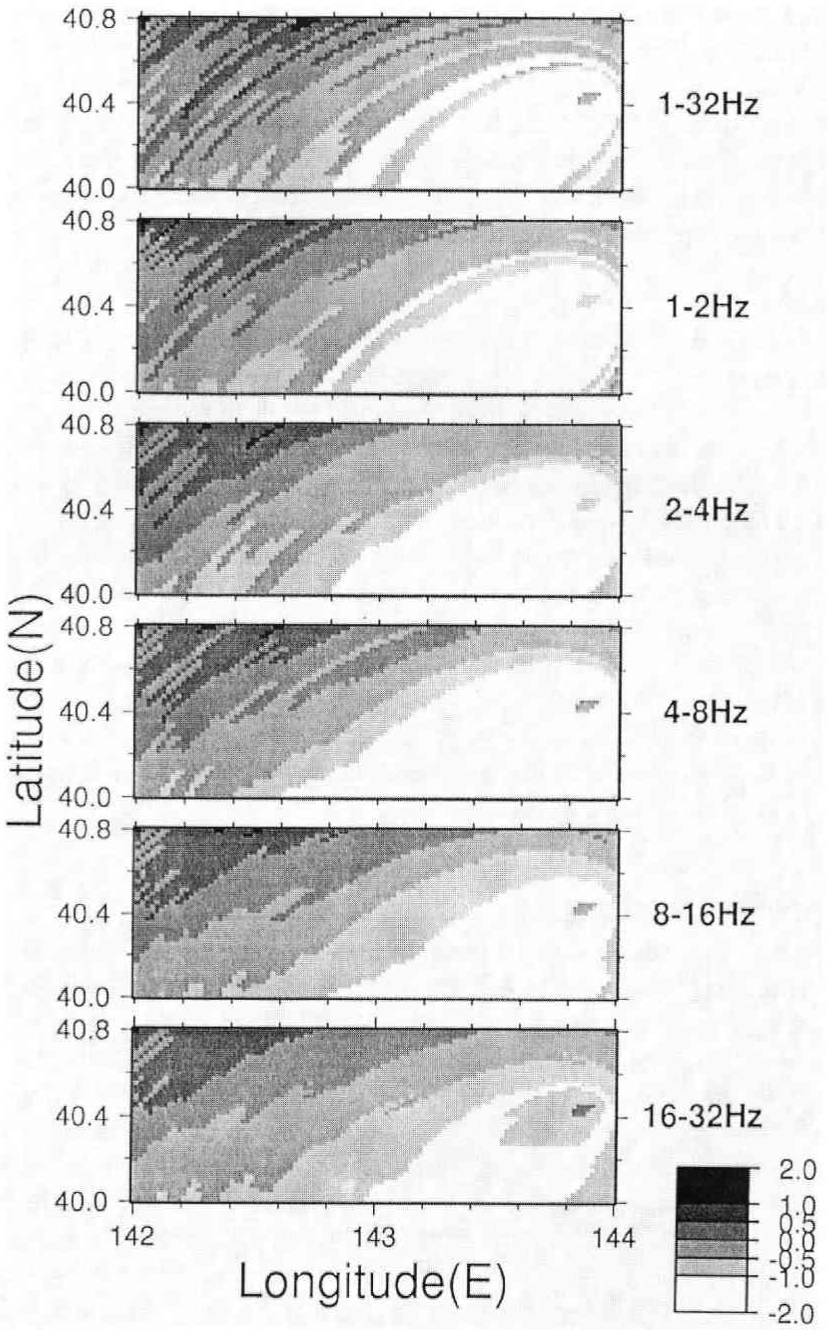

Fig. 6. Contour maps of the relative energy radiation intensity, RERI, for six frequency ranges. Darker shade represents stronger intensities. Scale is logarithmic, and the intensities are normalized by the average intensity for each frequency range.

the envelope consist of the waves radiated from plural subareas, we take the following steps to obtain a spatial distribution of the high-frequency wave radiation. First, we calculate squared velocity amplitude at a time and distribute them equally to the subareas where the isochrone intersects. Then, we estimate $r_a^2 e_l$ in eq.(3) correcting the effects of the hypocentral distance and the focal mechanism. We call $r_a^2 e_l$ as the *relative energy radiation intensity* (RERI). The spatial distribution of RERI shows the fault area where strong high-frequency waves are radiated from.

3.2. Result

By using the above method, we inverted the spatial distribution of RERI for six frequency ranges of 1-32, 1-2, 2-4, 4-8, 8-16, 16-32 Hz. We used the waveform data for 50 s, which corresponds to the time from the initial break to the rupture stopping, and calculated the isochrones and envelope seismograms at every 1 s. The results are shown in Figure 6, where dark shade represents high energy radiation and light gray does low radiation. For all the frequency ranges, it is found that radiation of high-frequency energy is strong in the western part of the fault. This means that the radiation of high frequency waves, initially having been weak, was accelerated with the westward propagation of fault rupture. The maximum intensity in the western region of the fault is as much as 100 times of that in and around the initial break. The patterns of spatial variation of the intensity seem to be smoother for the higher frequency ranges than lower frequency ranges, which may be due to the effect of source process and/or wave propagation in heterogeneous media. However, the resolution of our analysis is not high enough to distinguish those two possibilities.

4. Discussion and Conclusion

In Figure 7, we compare the intensity of high-frequency wave radiation for each subfault, slip distribution, and aftershock distribution for the first two weeks. The intensity of high-frequency waves is shown by RERI for the frequency range of 1-32 Hz. The amount of slip and the intensity of high-frequency waves are well correlated for the subfaults 3-8; the subfaults 3,4,6 have larger slips and stronger intensities, and the subfaults 5,7,8 smaller slips and weaker radiation. However, the subfaults 1 and 2, which are located at the western edge where the rupture stopped, indicate smaller slips and stronger radiation. Kosuga *et al.* (1995) also reported a strong energy radiation near the terminal of the fault from the analysis of arrival times of large amplitude waves in strong-motion records. The strong radiation may be a result of the high frequency waves radiated from rupture stopping area or places of large slip variation as suggested by Zeng *et al.* (1993) for the Loma Prieta earthquake. However, coda waves and reflection phases may partly affect the spatial distribution of high frequency wave radiation, therefore, it would be necessary to adopt a method taking heterogeneity of the structure into account for estimating more realistic distribution.

The largest aftershock (M=6.9) occurred in the subfault 1, where the slip was

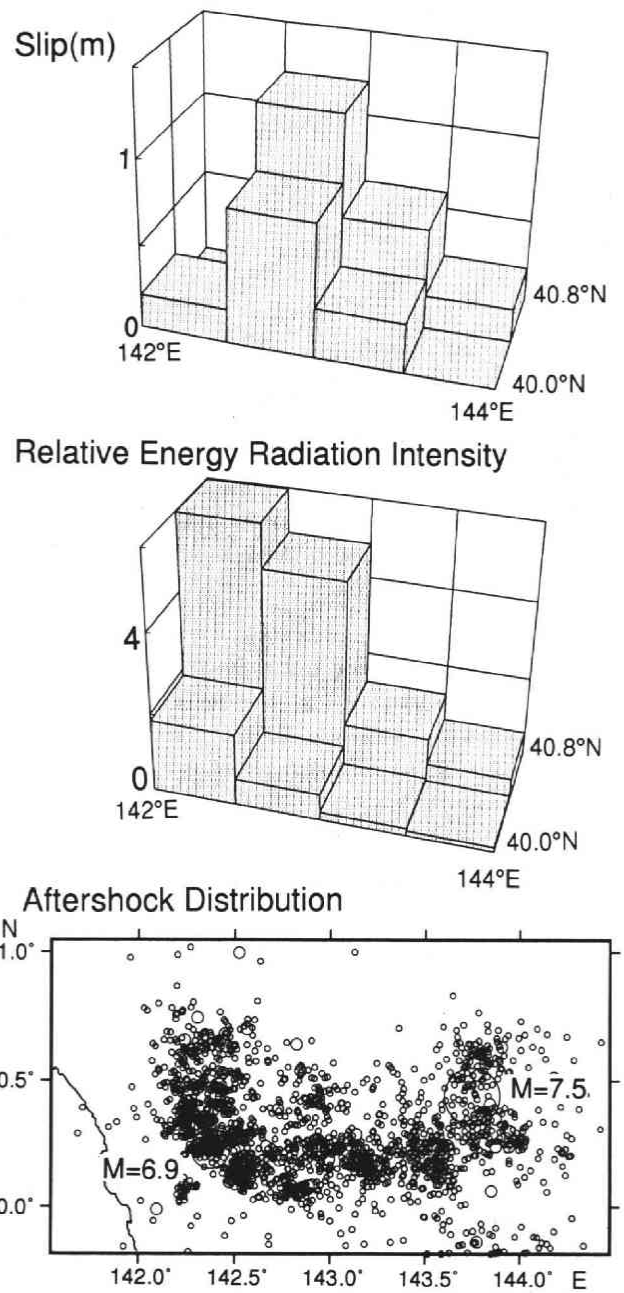

Fig. 7. Comparison of the aftershock distribution (Dec. 28, 1994–Jan. 10, 1995; after OCPEV) with the spatial distributions of the fault slip and relative energy radiation intensity, RERI.

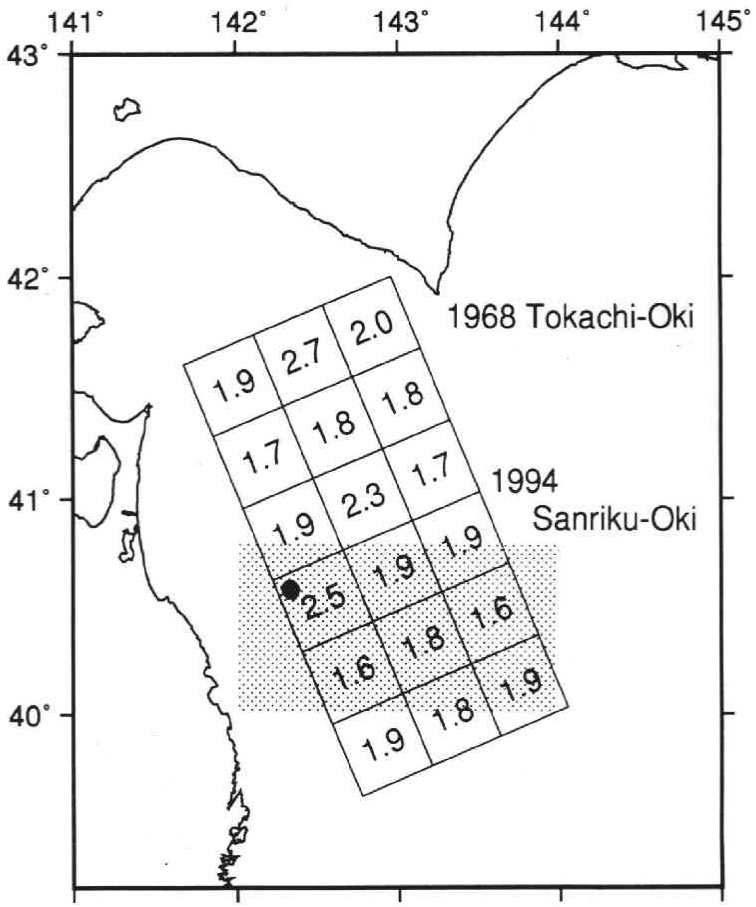

Fig. 8. Slip distribution of the 1968 Tokachi-Oki earthquake. Amount of slip is shown in each subfault with a unit of m. The solid circle denotes the midwestern subfault where larger slip is observed (see text). The data are read from Figure 11b of Mori and Shimazaki (1985). Shaded area represents the fault plane of the 1994 Sanriku-Oki earthquake.

smallest, 10 days after the main shock. Most of the aftershocks also took place in the region of small slip of the main rupture. On the contrary, a relatively small number of aftershocks were observed in the region of subfaults 4 and 6. Similar contrast is often seen in the source regions of other large earthquakes (e.g., Takeo, 1988).

The 1994 Sanriku-Oki earthquake took place in the area that was ruptured by the 1968 Tokachi-Oki earthquake (Ms=7.9). Figure 8 shows the slip distribution for the 1968 Tokachi-Oki earthquake after Mori and Shimazaki (1985) together with the source region of the 1994 Sanriku-Oki earthquake (see Fig. 1). Mori and Shimazaki (1985), analyzing Rayleigh waves with short period of 10-25 s, estimated the slip distribution by superposing the result on the averaged long-period slip by Kanamori (1971). Hence, it is necessary to note that the actual contrast of the slip distribution might be stronger

than that shown in the figure. In the figure, we recognize that the moment of the 1968 Tokachi-Oki earthquake was mainly released at two regions ; the midwestern edge and the northern edge of the fault. Comparing the spatial distribution of slip for the two large earthquakes, it is found that the fault area of the Sanriku-Oki earthquake shares southern part of the focal region of the Tokachi-Oki earthquake, where slip was relatively small. We, therefore, conclude that the 1994 Sanriku earthquake ruptured the portion of plate boundary where slip was incomplete at the time of the 1968 Tokachi-Oki earthquake of 26 years before. Figure 8 indicates a large slip (2.5 m) for the midwestern subfault of the Tokachi-Oki earthquake fault. This area roughly corresponds to the subfault 2 of the present study, where the moment release was nearly zero at the time of the 1994 Sanriku-Oki earthquake (see Fig. 7 and Table 1).

Mori and Shimazaki (1984, 1985) reported a good correlation between the spatial distributions of moment release and stress drop for the fault of the 1968 Tokachi-Oki earthquake. This is in good agreement with our result that the subfaults with large slip indicate strong radiation of high frequency waves for the 1994 Sanriku-Oki earthquake. At the subfault 2, however, the strongest radiation of high frequency waves is observed in spite of small slip of the fault.

The main result is summarized as follows :

(1) The fault of 170 km×84 km slipped mainly in the region from the middle to the western (landward) part, having the maximum slip of 1.2 m, whereas a small slip of less than 0.4 m was observed near the initial break point. The total seismic moment is estimated at 3.2×10^{20} Nm. The region of larger slip is characterized by low activity of aftershocks.

(2) The region of larger slip coincides with the region of low seismic moment release at the time of the 1968 Tokachi-Oki earthquake. This implies that the 1994 Sanriku-Oki earthquake completed the incomplete fault slip in the source region of the Tokachi-Oki earthquake.

(3) High-frequency wave energy was mainly radiated at the middle to western part of the fault rather than the initial break region, which is well correlated with the slip distribution. However, the western edge where the rupture stopped indicates strongest radiation of high-frequency waves but smaller low-frequency waves, suggesting generation of high-frequency waves associated with the termination of fault rupture.

Acknowledgments : We wish to thank the staff of the Observation Center for Prediction of Earthquakes and Volcanic Eruptions, Tohoku University, for providing us with hypocenter data of the main shock and aftershocks. We thank the Harvard University group for making available us the CMT solution through computer network. We are very grateful to Mr. and Mrs. Abe who kindly offered a part of their yard for the seismic observation.

References

Bouchon, M., 1981 : A simple method to calculate Green's functions for elastic layered media, *Bull. seism. Soc. Am.*, **71**, 959-971.

Kanamori, H., 1971 : Focal mechanism of the Tokachi-Oki earthquake of May 16, 1968 : Contortion at a junction of two trenches, *Tectonophysics*, **12**, 1-13.

Kennett, B.L.N. and N.J. Kerry, 1979 : Seismic waves in a stratified half space, *Geophys. J. R. astr. Soc.*, **57**, 557-583.

Kosuga, M., K. Imanishi, T. Sato, K. Tanaka and H. Sato, 1995 : Focal mechanism and rupture process of Sanriku-Haruka-Oki (off Sanriku) earthquake, *Investigation on the 1994 Sanriku-harukaoki earthquake and the earthquake disaster caused by it*, 79-88.

Matsuzawa, T., N. Umino, S. Horiuchi and A. Hasegawa, 1995 : Aftershock activity of the 1994 far east off Sanriku earthquake observed by a microearthquake observation network, *Abstract of 1995 Japan earth and planetary science joint meeting*, A31-08.

Mori, J. and K. Shimazaki, 1984 : High stress drops of short-period subevents from the 1968 Tokachi-Oki earthquake as observed on strong-motion records, *Bull. seism. Soc. Am.*, **74**, 1529-1544.

Mori, J. and K. Shimazaki, 1985 : Inversion of intermediate-period Rayleigh waves for source characteristics of the 1968 Tokachi-Oki earthquake, *J. Geophys. Res.*, **90**, 11374-11382.

Nishizawa, A., T. Kanazawa, T. Iwasaki and H. Shimamura, 1992 : Spatial distribution of earthquakes associated with the Pacific plate subduction off northeastern Japan revealed by ocean bottom and land observation, *Phys. Earth Planet. Interiors*, **75**, 165-175.

Spudich, P. and L.N. Frazer, 1984 : Use of ray theory to calculate high-frequency radiation from earthquake sources having spatially variable rupture velocity and stress drop, *Bull. seism. Soc. Am.*, **74**, 2061-2082.

Takeo, M. 1988 : Rupture process of the 1980 Izu-Hanto-Toho-Oki earthquake deduced from strong motion seismograms, *Bull. Seism. Soc. Am.*, **78**, 1074-1091.

Umino, N., T. Matsuzawa and A. Hasegawa, 1995 : Focal depth distribution of aftershocks of the 1994 far east off Sanriku earthquake estimated from sP phases, *Abstract of 1995 Japan earth and planetary science joint meeting*, A31-09.

Zeng, Y., K. Aki and T. Teng, 1993 : Mapping of the high-frequency source radiation for the Loma Prieta earthquake, California, *J. Geophys. Res.*, **98**, 11981-11983.